Sensors & Actuators: B. Chemical 464 (2026) 140134

Contents lists available at ScienceDirect

Sensors and Actuators: B. Chemical

journal homepage: www.elsevier.com/locate/snb

Discrimination for fifteen genotypes of human papillomavirus (HPV) via multiplexed qPCR in a portable and automated device

Jingyang Zhao [a,b,1], Yingjun Xiao [c,1], Jiajun Li [a], Chao Liang [a,*], Hanqing Jiang [a,d,e,**]

[a] School of Engineering, Westlake University, Hangzhou, Zhejiang 310030, China
[b] School of Materials Science and Engineering, Zhejiang University, Hangzhou, Zhejiang 310027, China
[c] The Third Affiliated Hospital of Zhejiang Chinese Medical University, Hangzhou, Zhejiang 310009, China
[d] Research Center for Industries of the Future, Westlake University, Hangzhou, Zhejiang 310030, China
[e] Westlake Institute for Advanced Study, Hangzhou, Zhejiang 310024, China

ARTICLE INFO

Keywords:
HPV screening
Point-of-Care testing
Multiplexed qPCR
Rigid-flexible pneumatic switching

ABSTRACT

Screening for human papillomavirus (HPV) genotypes is crucial for cervical cancer prevention and has gained widespread attention. However, a comprehensive discrimination of all the high-risk HPV (hr-HPV) is still limited to centralized facilities, where testing is time-consuming, costly, and only performed by trained specialists. Although many point-of-care testing (POCT) platforms have been developed, they currently monitor only a limited number of hr-HPV genotypes (mainly HPV16 and HPV18) and suffer from poor detection accuracy. Here, we report a portable and automated POCT platform that is capable of simultaneously identifying fifteen genotypes of HPV, including all fourteen hr-HPV genotypes and one type of possibly high-risk HPV (phr-HPV). The platform features a rigid-flexible pneumatic switching (RFPS) technology, which can automatically perform omnidirectional dispensing, on-demand releasing, vortex mixing, and long-term storage of multiple reagents in a palm-sized cartridge. A compact benchtop device, about the size of a shoebox, with a movable fluorescence detection module, has been developed for 4 × 4 quantitative real-time polymerase chain reaction (qPCR). By using the platform, we achieved a limit of detection (LOD) of 3∼50 copies/μL for all fifteen HPV subtypes. Validated by 53 clinical samples, the platform successfully delivered "sample-in-answer-out" performance in one hour, demonstrating good concordance with a gold standard analyzer (Pearson coefficients = 0.94), with 96.4% sensitivity and 96% specificity. This platform not only advances HPV screening but also expands a range of POCT technologies with strong potential for commercialization.

1. Introduction

Cervical cancer ranks as the fourth most common cancer among women, with an estimated 600,000 new cases and more than 300,000 deaths each year, accounting for 7% of all female cancer cases worldwide [1]. Almost all of the cervical cancer cases (more than 95%) can be attributed to the infection of human papillomavirus (HPV) [2,3]. HPV belongs to a large papillomavirus family with more than 200 genotypes, which includes 14 types of high-risk HPV (hr-HPV) that can cause cervical lesions [4] and low-risk HPV (lr-HPV) that are merely associated with genital warts [5]. Recent studies have shown that a single infection of some HPV (especially HPV 73) with high viral loads can also lead to cervical cancer [6–8]. Such types are categorized as possibly high-risk HPV (phr-HPV). Although the hr-HPV subtypes of HPV 16 and 18 account for over 70% of all cervical cancers in the United States [9], only HPV 16 and 18 results are not enough for cervical cancer screening since the other hr-HPV and phr-HPV infections can cause different cervical cancer distributions in other countries and may vary at different periods within the same region [10]. Therefore, a comprehensive screening of all the hr-HPV and some phr-HPV (such as HPV 73) is crucial for the prevention of progression from treatable HPV infection to severe cervical cancer.

Various methods have been developed for HPV screening, including Papanicolaou (Pap) test [11], lateral flow assays (LFA) [12,13], isothermal amplification techniques [14–16], reverse dot blots [17], and CRISPR-Cas-based analysis methods [18–20]. However, in terms of

* Corresponding author.
** Corresponding author at: School of Engineering, Westlake University, Hangzhou, Zhejiang 310030, China.
E-mail addresses: liangchao@westlake.edu.cn (C. Liang), hanqing.jiang@westlake.edu.cn (H. Jiang).
[1] These authors contributed equally to this work.

https://doi.org/10.1016/j.snb.2026.140134
Received 7 November 2025; Received in revised form 21 April 2026; Accepted 7 May 2026
Available online 9 May 2026

precision and robustness, these methods still cannot fully replace quantitative real-time polymerase chain reaction (qPCR), which is the most commonly used method and regarded as the clinical "gold standard" [21,22]. However, qPCR comes with challenges: it requires a bulky robot arm to transport reagents between different reaction steps, multiple fluorescence detection modules for multiplexed signal emission and reading, and trained specialists to pre-load reagents, operate, and maintain the complex instrument, making it restricted to centralized facilities. In fact, 56% of women in low- and middle-income countries (LMICs) have never been screened for cervical cancer during their lifetime [23]. Decentralized point-of-care testing (POCT) is critical for effective cervical cancer prevention, especially in LMICs, since it is capable of early and immediate treatment of HPV infection at the patient's site.

According to the World Health Organization (WHO), an ideal POCT should be ASSUATED: Affordable, Sensitive, Specific, User-friendly, Rapid and robust, Equipment-free, and Deliverable to end users [24]. To meet these criteria, a multiplexed POCT device needs to handle several functions: omnidirectional dispensing (to manage multiple reagents operation without manual intervention), on-demand releasing (to proportionally control reagent flow for accurate testing results), long-term storage (to avoid reagents pre-loading), and a simple design (to ensure cost-effectiveness and robustness). However, most current POCT approaches cannot simultaneously satisfy all these features [25–27]. As a result, they often detect only a limited range of HPV subtypes (mostly HPV 16 and 18) with poor detection accuracy. For example, the capillary-driven [28,29] and gravity-driven [30,31] POCT devices only perform one-directional reagent transportation, limiting their application to multiple reagents operations. CD-like microfluidic devices [32–35] actuated by centrifugal forces suffer from their complicated siphon networks, and the inertia force generated by the high-speed motor may result in unintended flow behavior, thereby decreasing their operational accuracy. The precision and repeatability of finger-actuated POCT devices [36–38] could be compromised by slight variations in the activities of different users. Pneumatic POCT devices [39–42] exhibit fast, precise, and versatile capabilities for multiple reagent handling; however, several separate pneumatic channels must be applied to adjust each pneumatic valve, increasing system complexity and compromising its robustness. More importantly, none of the POCT technologies mentioned above exhibit long-term reagent storage capability, as the reagents must be manually added to the chamber by end-users before application.

Here, we present a portable and automated platform for discrimination of fifteen HPV variants (including all fourteen types of hr-HPV and one type of phr-HPV) via multiplexed qPCR. The platform comprises a parm-sized cartridge and a benchtop device. The cartridge features a rigid-flexible pneumatic switching (RFPS) technology, which is capable of self-regulated the applied pressure without the need of extra pneumatic adjusting channels, automatically performing omnidirectional dispensing, on-demanding releasing, vortex mixing and long-term storage of multiple reagents (Fig. 1A). The benchtop device simplifies multiple fluorescence detection modules to a single movable module for 4 × 4 qPCR (Fig. 1B), significantly reducing both cost (see Supplementary Table 1) and overall size (comparable to a shoebox). With this platform, a limit of detection (LOD) of 3–50 copies/μL for all fifteen HPV subtypes can be achieved. Validated by 53 clinical samples, the platform achieved "sample-in-answer-out" performance in one hour, demonstrating good concordance with a gold standard analyzer (Pearson coefficients = 0.94), along with 96.4% sensitivity and 96% specificity. Compared with existing POCT technologies (Table 1), our platform offers the most comprehensive HPV screening (Fig. 1C) with clinically applicable accuracy (Figs. 1D and 1E). Although our platform still need a portable device to achieve multiplexed readouts, compared with the commercial POCT platform (such as GeneXpert Xpress), it shows advantages in terms of multiplexed detection capability, affordability and portability, which demonstrates strong potential to improve accessibility and effectiveness of HPV screening, particularly in LMICs.

2. Experimental section

2.1. Materials and reagents

DNA extraction reagents of HPV, including beads, wash, and elution buffer, were purchased from Wuxi Donglin Sci & Tech Development Co., Ltd. Primers, probes, Taq polymerase, and the amplification basis for the 14 high-risk HPV and 1 phr-HPV discrimination were provided by Liferiver Bio-Tech Corp. Standard samples with known concentrations and Tris-EDTA buffer solution for calibration were purchased from also Liferiver Bio-Tech Corp. Paraffin oils applied for sealing the waste chamber and amplification tubes were purchased from Sinopharm Chemical Reagent Co., Ltd. All reagents were prepared and stored according to the manufacturer's specifications to ensure optimal performance during the PCR and sequencing steps. TPU film was purchased from Xinrui (China), adhesives 9731 from 3 M (USA), and the 3D-printing material polylactic acid (PLA) from Raise3D (China).

2.2. Design and fabrication of the RFPS cartridge

Cartridge substrate and cover were designed by using AutoCAD 2023 and Solidworks 2019. The RFPS consists of a block on the substrate, an elastic film, and a lever connected to the cover via a hinge, resulting in an interference fit when assembled. Y-shaped clip structures are used in the cover layer to assemble the RFPS. The Y-shape clip has a clearance between two legs. When the clip is pushed into the groove, the two legs bend slightly and then recover to its original state as it comes through the groove and tightly binds the cover and the substrate. The detailed dimension information is provided in Supplementary Figure S1. The cartridge was fabricated through an Ender 3 Pro 3D printer (Shenzhen Creality 3D Technology Co. Ltd.). After printing, the surface of the substrate layer was polished using 800-grit sandpapers (3 M, 407Q), reducing surface roughness from about 24 μm to below 0.1 μm. The surface roughness is measured using a surface profilometer (KLA-Tencor, USA) and the results are provided in Supplementary Figure S2. Double-sided adhesive films were cut using a Silhouette Cameo 2 cutter (Silhouette America, Inc.). The TPU film was bonded to the substrate layer using the adhesives by hot pressing at 45 ℃ for 10 min. Finally, the cover was applied to the substrate layer through the mechanical clamper. Photos of the cartridge components are provided in Supplementary Figure S3.

2.3. Flow behavior test for the RFPS cartridge

Images of omnidirectional dispensing and on-demand performances were captured using a high-speed camera (Revealer NEO 25 with a frame rate of 16000fps). An air compressor was used to generate the air pressure, and several digital precision pressure regulators were used to adjust the pressure value. The flow behavior testing process is as follows. A given amount of liquid was injected into the testing device, and a high-speed camera was used to record the flow behavior. Still images were then extracted from the flow behavior video at fixed time points, and the remaining area was calculated using Image-Pro Plus software. The computed area was then multiplied by the chamber depth to determine the volume. Details on the flow behavior testing system can be found in Supplementary Figure S4.

The vortex mixing tests were performed as follows. A 250 μL testing liquid deionized (DI) water, ethanol, and glycerol) with 50 μL microbeads was injected into a cartridge. Mixing performance was recorded with a high-speed camera at 0.1 s intervals under a pressure of 4 kPa. Pixel information during mixing was extracted from these images using Photoshop CS6, and the mixing efficiency M was calculated according to the following equation (43).

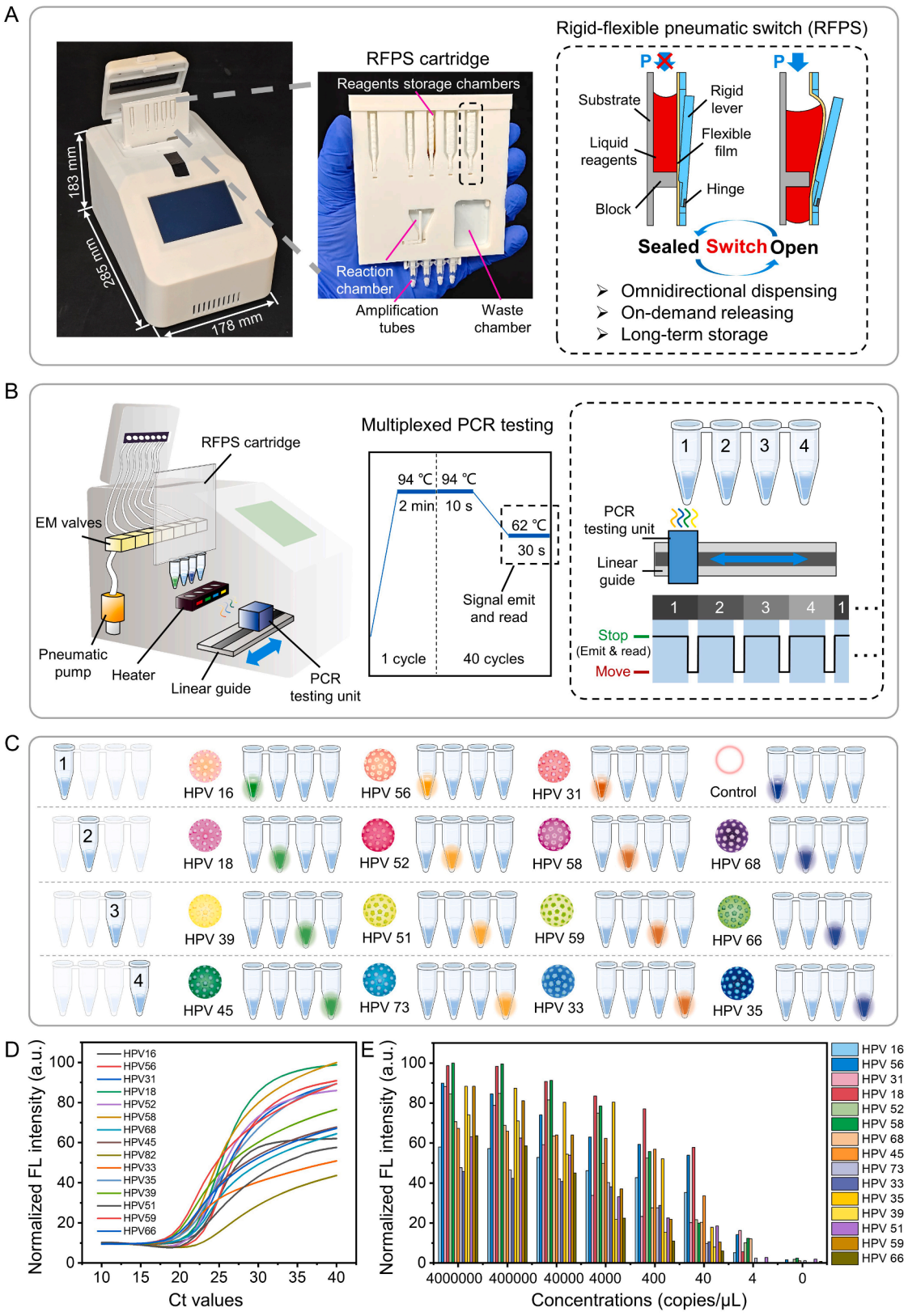

Fig. 1. Overview of the multiplexed POCT platform for HPV identification. (A) Images of a cartridge with rigid-flexible pneumatic switches (RFPS), which enables omnidirectional dispensing, on-demand releasing, and long-term storage of reagents. (B) Schematic diagram of a portable and automated device, which is capable of conducting 4 × 4 multiplexed qPCR testing with a single movable PCR testing unit. (C) Schematic diagram of the multiplexed qPCR testing in four tubes for 15 HPV genotypes. (D) and (E) Testing results for 15 HPV genotypes using the POCT platform.

Table 1
Comparison of current methods for point-of-care testing of HPV.

	This work	Cai et al. (2024) [19]	Zhao et al. (2021) [15]	Xu et al. (2025) [18]	Xu et al. (2022) [20]	Seely et al. (2023) [13]
HPV genotypes	15 types	2 types	5 types	2 types	9 types	14 types
Reaction methods	qPCR	CRISPR	LAMP	CRISPR	CRISPR	LAMP
Limit of detection	3–50 copies/μL	10^{-18} M	10^{3} copies/μL	10^{-18} M	2.6 x 10^{-19} M	10 copies/ reaction
Sensitivity	96.4%	100%	91.7%	95.6%	97.8%	93%
Specificity	96%	95.8%	100%	100%	98.1%	73%
Sample pre-treatment	No (on-chip auto purification)	Yes (manual pre-treatment)	No (on-chip auto purification)	Yes (manual pre-treatment)	Yes (manual pre-treatment)	Yes (manual pre-treatment)
Turn-out time	63 min	30 min	40 min	50 min	40 min	30 min

$$M = 1 - \sqrt{\frac{1}{N}\sum_{i=1}^{N}\left(\frac{c_i - \bar{c}}{\bar{c}}\right)}$$

where N is the total number of sample pixel points, c_i and $\bar{c}$ are the normalized concentration and expected normalized concentration, respectively. Mixing efficiency ranges from 0 (0%, not mixing) to 1 (100%, full mixed).

For the long-term storage tests, the reagent storage chambers of the cartridge were filled with the DNA extraction reagents, and the reagent loading ports were sealed with a cover. The cartridges were then stored at 25 °C and 45 °C, respectively. Their weight was measured and recorded every seven days. Three independent experiments were conducted with the data shown as ± s.d.

2.4. Preparation of clinical sample testing

The collection and use of cervical swab samples were approved by the ethics committee of the Third Affiliated Hospital of Zhejiang Chinese Medical University (No. ZSLL-ZN-024–028–01) and Westlake University (No. 20241101JHQ001). The participants are all volunteered to be tested with no compensation. After the cervical swab samples were collected, each was labeled with a unique identifier and immediately placed in a 2 mL preservative solution to maintain the integrity of the nucleic acids and prevent degradation. The samples were stored at −40°C for conventional qPCR and RFPS-POCT platform procedures.

2.5. Conventional qPCR procedures for comparison experiments

The DNA extraction and amplification reagents were prepared as follows. First, 6 μL of AcrylCarrier and 20 μL of magnetic microbeads were added to 500 μL of bonding buffer solution, which was then shaken to yield a 526 μL microbead solution. Next, 21 mL of ethanol was added to washing solutions A and W, which were then shaken. After shaking, washing solutions A and W were obtained, respectively. Finally, 36 μL of HPV nucleic acid fluorescence PCR testing mixture was combined with 0.4 μL of Tag enzyme, shaken, and centrifuged for several seconds, producing the amplification reagents for multiplexed qPCR.

526 μL microbead solution was pipetted into a 1.5 mL centrifuge tube, where a 200 μL sample was added. The tube was then manually shaken up and down 10 times. The 726 μL mixture was transferred to the affinity column, where it was centrifuged for 60 s at a rotation speed of 13,000 rpm. The waste solution was then abandoned. 500 μL of washing solution A was added to the affinity column, and centrifugation was performed for 40 s at a rotation speed of 13,000 rpm. The waste solution was subsequently discarded. This washing process was repeated twice. 500 μL of washing solution W was added to the affinity column, followed by centrifugation for 15 s at a rotation speed of 13,000 rpm. The waste solution was then discarded. This washing process was also repeated twice. A 200 μL elution solution was added to the affinity column, followed by centrifugation for 2 min at a rotation speed of 13,000 rpm. The elution solution was added to 36 μL of amplification solution in the PCR tube, which was then placed in a real-time PCR testing equipment (SLAN-96P) to perform the qPCR process. The qPCR temperature profile can be found in Fig. 1B. The entire testing process took approximately 150 min (DNA extraction was 30 min, and qPCR testing was 120 min).

2.6. RFPS-POCT platform configuration

A total of 526 μL of microbeads solution, 1000 μL of washing A solution, 1000 μL of washing W solution, 200 μL of elution solution, and 700 μL of paraffin oils were pre-loaded into the lysis chamber, washing1 chamber, washing2 chamber, elution chamber, and paraffin chamber of the cartridge, respectively. Then, the reagent loading ports were sealed with a cover, allowing the cartridge to be stored long-term and readily delivered to end-users. Upon receiving the cartridge, users only need to add 200 μL of sample to the lysis chamber and insert the cartridge into the detection device, where the DNA extraction and PCR procedures are pre-programmed (Supplementary Figure S5). After about 60 min, the testing results can be obtained.

3. Results and discussion

3.1. Multiplexed qPCR for fifteen types of HPV variants

The design of forward and reverse primers, as well as probes, is crucial for achieving high specificity and sensitivity in multiplexed qPCR assays. The primers were designed to target conserved regions, specifically the L1 open reading frame of the HPV genome, which is highly conserved across different HPV types (Figs. 2A and 2B). The length of the primers ranges from 25 to 30 nucleotides, with optimized melting temperature (T_m) between 55 °C and 68 °C to ensure efficient annealing. The guanine-cytosine (G-C) content of the primers is typically between 40% and 60%, which balances stability and specificity, thereby avoiding secondary structures and self-complementarity. The probes are designed to be complementary to the region within the amplified sequences, in HPV variant L1 regions between 6500 and 6800 (Fig. 2C). Probes are labeled with fluorescent dyes, FAM, VIC, Texas Red, and Cy 5, and a quencher molecule to enable the detection of the amplified DNA at 62 °C. The probe designs are validated to prevent potential secondary structures and to ensure that it does not form dimers with the primers. Taq polymerase, $MgCl_2$, dNTPs, and other necessary components are added to the reagent to create a proper salt environment and provide the required material for amplification. In the 4 × 4 multiplex system, each genotype was detected using the same set of four primers, comprising two forward and two reverse, as a redundant design to enhance amplification robustness. The allocation of genotypes among the four tubes was optimized to separate the most locally similar targets across different reactions, for example, shared target-region motifs between HPV56/66, HPV16/52, HPV52/33, and HPV59/35. This design helped minimize cross-reactivity and maintain clear signal discrimination. By

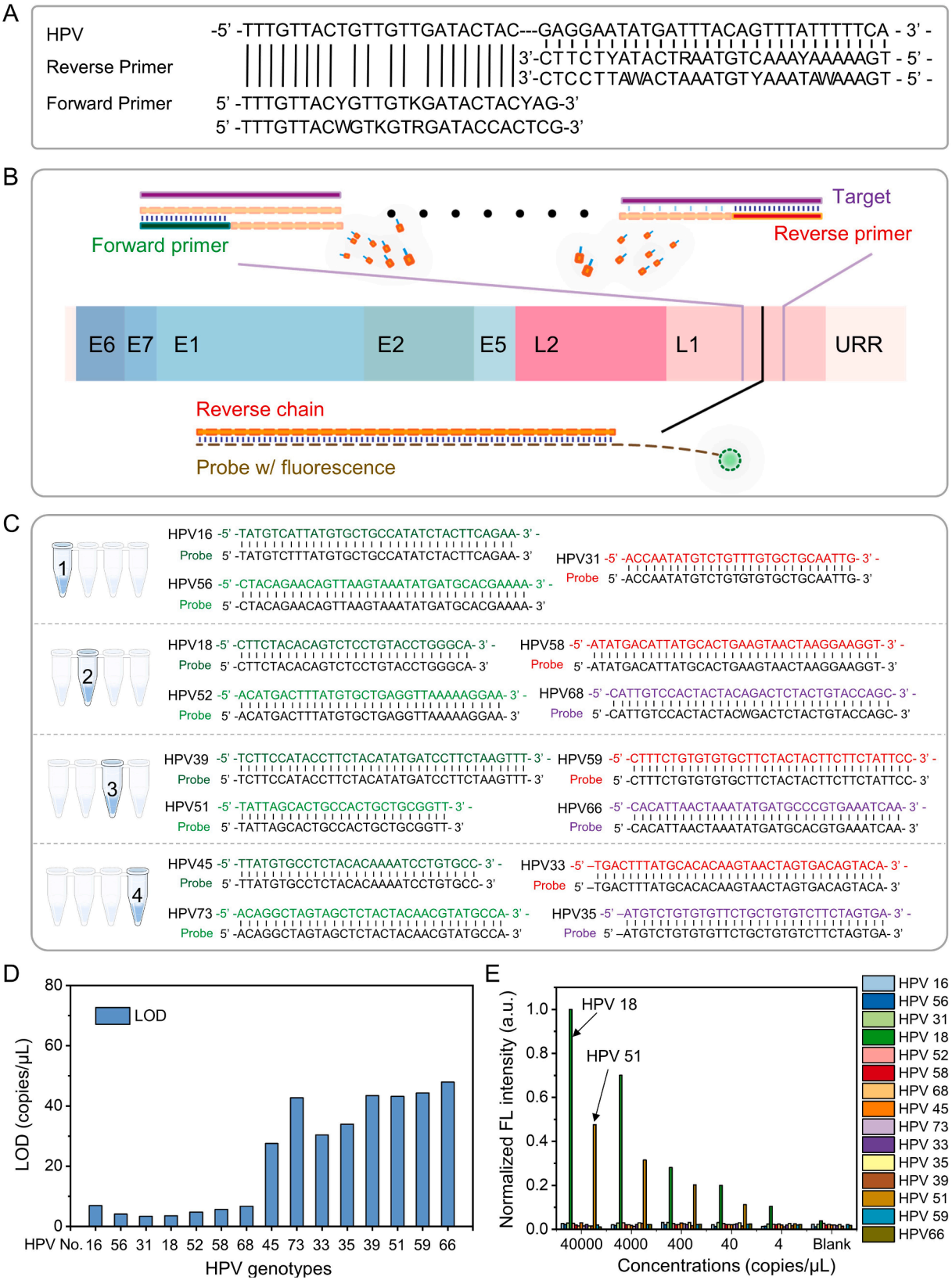

Fig. 2. Identification of HPV types by multiplexed qPCR. (A) Sequences of original HPV and amplification primers. (B) Schematic diagram of target sites in HPV DNA and primer pairs designed for multiplex qPCR. (C) Sequences of DNA probes in HPV panel. (D) Limit of detection (LOD) of 15 types of HPV. (E) HPV 18 and HPV 15 genotypes identification in all the 15 types of HPV from 4000000 copies/μL to 400 copies/μL.

using the multiplexed qPCR strategy, the limit of detection (LOD) for all fifteen HPV genotypes was below 50 copies/μL, among which HPV 31 achieved the lowest LOD of 3.3 copies/μL and HPV 66 exhibited the highest LOD of 47.9 copies/μL (Fig. 2D). Fig. 2E clearly demonstrated the capability in viral discrimination, where HPV 18 and HPV 51 can be successfully identified among the fifteen types of HPV genotypes with their concentration even decreasing to 4 copies/μL.

3.2. Characterization of the RFPS cartridge

Fig. 3A shows the dimensions of the RFPS cartridge (Length = 125.5 mm, Width = 96.5 mm, and Thickness = 8 mm), which comprises four layers: substrate layer, adhesive layer, elastic film, and cover (Fig. 3B). Fig. 3C demonstrates the chamber arrangement in the RFPS cartridge, including the reagent storage chambers, pushing channel, mixing channel, reaction chamber, waste chamber, and amplification tubes. The paraffin oil, elution reagent, lysis solution, washing A solution, and washing W solution were pre-added and stored in the respective reagent storage chambers. When the users received the cartridge, they only needed to remove the sealing cover, add the sample, insert it into the benchtop device, and wait for the test results. Several RFPSs are arranged at the inlet/outlet to the reaction chamber (red circle in Fig. 3C), which enables omnidirectional dispensing, on-demand releasing, vortex mixing, and long-term storage of multiple reagents.

Fig. 3D illustrates the mechanism of RFPS. In the absence of pneumatic pressure, the hinge bends due to the interference fit, and the lever applies a sealing force F_S' that presses the elastic film against the block, keeping the liquid sealed in the chamber (sealed state). When the pressure is applied to the chamber, the elastic film expands outward through the cover layer and pushes the lever upward. Once the pressure exceeds the critical pressure P_c, the interference fit is overcome, a gap opens at the end of the lever, and the reagent in the chamber flows into the next chamber. Based on the simple lever principle, it can be seen that as the length of the lever increases (lever width = 3 mm, lever thickness = 2 mm), the critical pressure decreases. Experimentally, the critical pressure was 38.3 ± 2.1 kPa for a lever length of 16 mm, and dropped to 18.1 ± 2.8 kPa when the lever length was increased to 58 mm (three independent experiments, data shown as ± s.d.). We tested the influences of lever thickness and width on the critical pressure and the results are provided in Supplementary Figure S6. It can be seen that the critical pressure was about 30 kPa when the lever thickness was 1 mm (lever length = 40 mm, lever width = 2 mm). As the lever thickness increased from 2 mm to 4 mm, the critical pressure was almost the same (decreasing to about 23 kPa). As the lever width varied from 1 mm to 2 mm (lever length = 40 mm, lever thickness = 2 mm), the critical pressure was also remaining the same. It can be observed an obvious deformation of the lever when its thickness was 1 mm and thus it needs a larger force to push the lever up for reaching the critical pressure. When the stiffness of the lever was sufficient (thickness more than 2 mm), no lever deformation was observed and the relationship between lever dimension and critical pressure follows the lever principle, where the lever balance only depends on the lever length and the force exerted on the lever. The green star in Fig. 3D shows the length of actual lever (37 mm) and the critical pressure (23 kPa) used in the cartridge. It can be seen that the actual lever data fit the curve quite well, which means the curve can provide an important basis for the design of cartridge. It is important to note that the RFPS is capable of self-regulating the critical pressure by adjusting the length of the lever, making it readily achievable to transport the selective reagent to different chambers. Compared to current pneumatic POCT devices, the RFPS-POCT device does not require additional pneumatic channels to control the open/close state of the pneumatic valves, thereby dramatically reducing its complexity and enhancing its robustness.

Fig. 3E exhibits the selective transportation performance of the RFPS cartridge. When pressure P1 (P1 < PC) was applied to the reaction chamber through the pushing channel, the block of the RFPS prevented reagents from entering the amplification tubes, but instead directed them into the waste chamber. When both P_1 and P_2 ($P_1 + P_2 > P_C$) were simultaneously applied, the lever of the RFPS was lifted and the reagents flowed into the amplification chamber. In this way, the flow behavior can be readily switched between different chambers. It should be noted that when pressure was removed, the flow can be immediately stopped, due to the quick elastic recovery of the hinge, which pushes the lever back to the block and thus seals the chamber. As shown in Fig. 3F and Movie S1, when pressure was released every 2 s, flow stopped immediately at each cycle, demonstrating the cartridge's on-demand releasing capability.

Supplementary material related to this article can be found online at doi:10.1016/j.snb.2026.140134.

When the pressure is applied to the bottom of reaction chamber through mixing channel, the air bubble can generate an efficient vortex mixing. Tests were performed with liquids of different viscosities and surface tensions. As shown in Fig. 3G, ethanol (viscosity of 1.2 mPa·s, surface tension of 22.3 mN/m) and DI water (viscosity of 1.0 mPa·s, surface tension of 72.8 mN/m) reached complete mixing in about 4 s under 4 kPa. For glycerol (viscosity of 1500 mPa·s, surface tension of 63.3 mN/m), it took 22 s to complete thorough mixing at a pressure of 4 kPa, but only 9 s when the pressure was increased to 10 kPa. Vortex mixing video is provided in Movie S2. The current microfluidic mixing technologies mostly rely on two strategies: one is the continuous flow of the fluid to be mixed through serpentine microchannel [43] or obstacles [44], and the other one is entire liquid volume to be mixed by shaking [45] or reciprocation [46]. However, the Euler force in these mixing technologies may not be strong enough to cause a sloshing of the liquids and the internal fluid flows are not strong enough to cause rigorous mixing of the two fluid phases, resulting in a low mixing efficiency especially for the liquid with high viscosity [47]. In our method, the air bubbles are inserted from the bottom of the reaction chamber and rise due to buoyancy force, thereby inducing a robust drag flow and mixing of the entire fluids. And the rupture of the air bubbles will occur leading to vigorous turbulence mixing. Therefore, the RFPS cartridge demonstrated higher efficiency (full mixing within several seconds), simplicity (only need a pneumatic channel at the bottom of the reaction chamber), and broader applicability across different liquids (even viscosity as high as 1500 mPa·s).

Supplementary material related to this article can be found online at doi:10.1016/j.snb.2026.140134.

Fig. 3 H showed the long-term storage performance of the cartridge. After 84 days, reagents weight decreased by only 1.2% at 25 °C and 3.6% at 45 °C. Before the elution step, it is necessary to perform a drying step since the residual ethanol from the washing steps can strongly inhibit the activity of DNA polymerase and other enzymes, resulting in PCR amplification failure or low yield. Common drying methods, such as low-temperature heating and high-speed centrifugation, are time-consuming (usually several minutes) and need extra equipment (heater and centrifuge). In the RFPS cartridge, the drying step was performed by introducing air pressure to the bottom of the reaction chamber. Fig. 3I exhibits the relationship between drying time and Ct value with the air pressure of 30 kPa. It can be seen that there were no Ct values when no drying step and drying time of 5 s were applied. As the drying time varied from 10 s to 20 s, the Ct values decreased from 37 to 28 and the Ct values almost remained the same when the drying time increased to 25 s. The A260/A230 tests were also performed using UV-Vis Spectrophotometer (Thermo Scientific NanoDrop), where A260 is the absorbance peak of DNA/RNA and A230 is the absorbance peak of impurities such as organic solvents. It can be seen that the A260/A230 value with the drying time of 20 s was 2.1 which was within the normal range of 1.8–2.2. The A260/A230 value was 1.3 without the drying process, indicating some pollutants (such as ethanol in the washing solutions) remaining in the chamber and disturbing the amplification reaction.

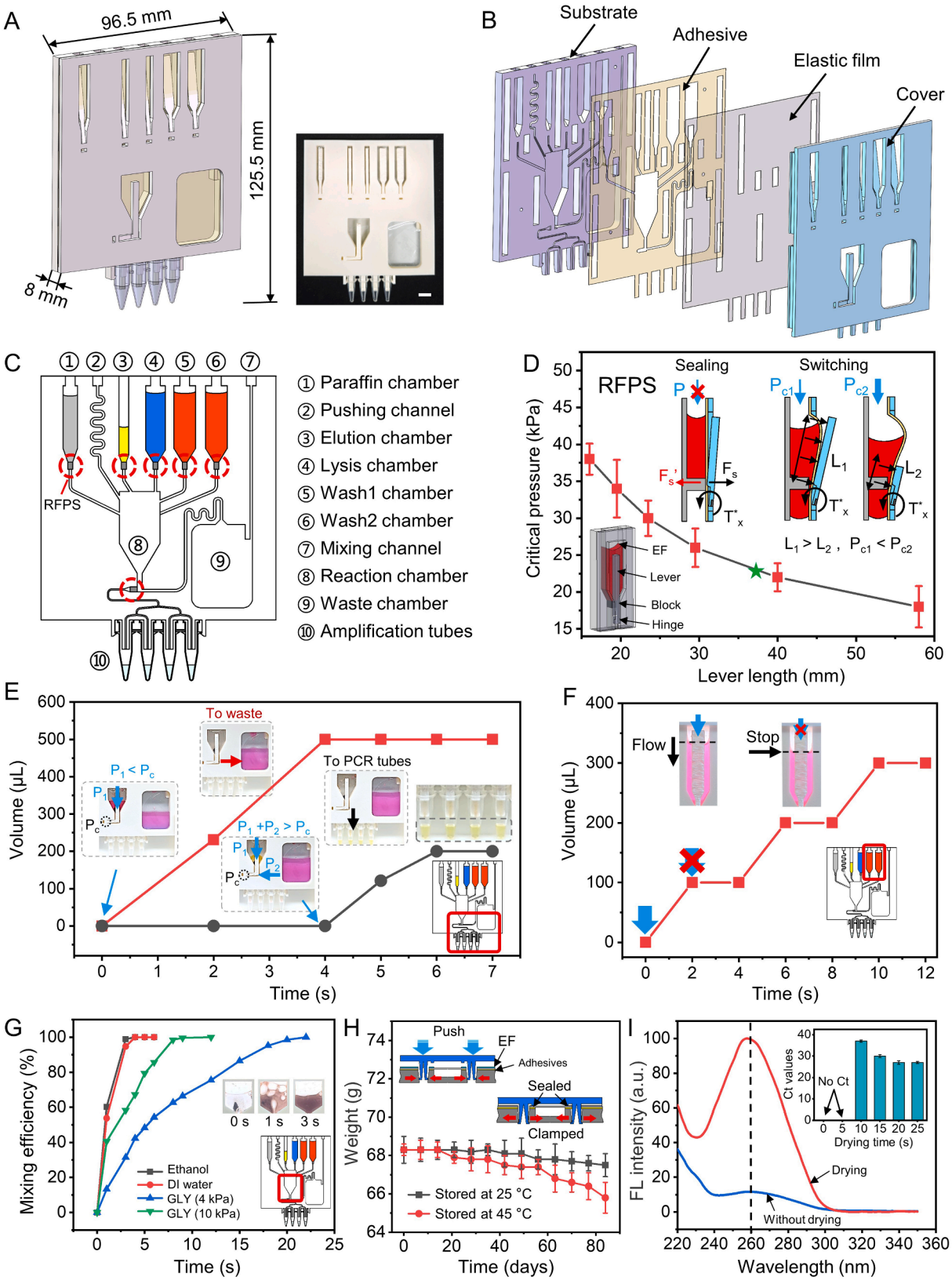

Fig. 3. Characterization of RFPS cartridge. (A) Schematic diagram of RFPS cartridge demonstrating its dimension. The insert is a picture of the cartridge with the scale bar of 1 cm. (B) Expanded view schematic diagram of RFPS cartridge. (C) Schematic diagram showing the chamber function of RFPS cartridge. (D) The relationship between the lever length and the critical pressure. The green star represents the actual lever length and critical pressure of the cartridge. The insert shows the mechanism of RFPS. (E) Omnidirectional dispensing performance of RFPS cartridge, where liquid is capable of selectively transporting to waste chamber and PCR tubes. (F) On-demand releasing performance which can precisely control the volume of releasing liquid. (G) Mixing performance in RFPS cartridge. (H) Reagents storage testing results. (I) The influence of drying process for amplification results in RFPS cartridge. The insert presents the relationship between Ct values and drying time.

3.3. Performance of the benchtop device

Fig. 4A showed the internal structure of the benchtop device. The device consists of a pneumatic module, a heating/cooling module, and a fluorescence module. The pneumatic module includes an electromagnetic switch to control pneumatic pressure open/close state, an electromagnet to capture the microbeads in the reaction chamber, and an air pump to generate the required pressure. The heating/cooling module is composed of a Peltier heating plate, a temperature sensor, an aluminum heat sink, and a fan. The heating area is specifically designed

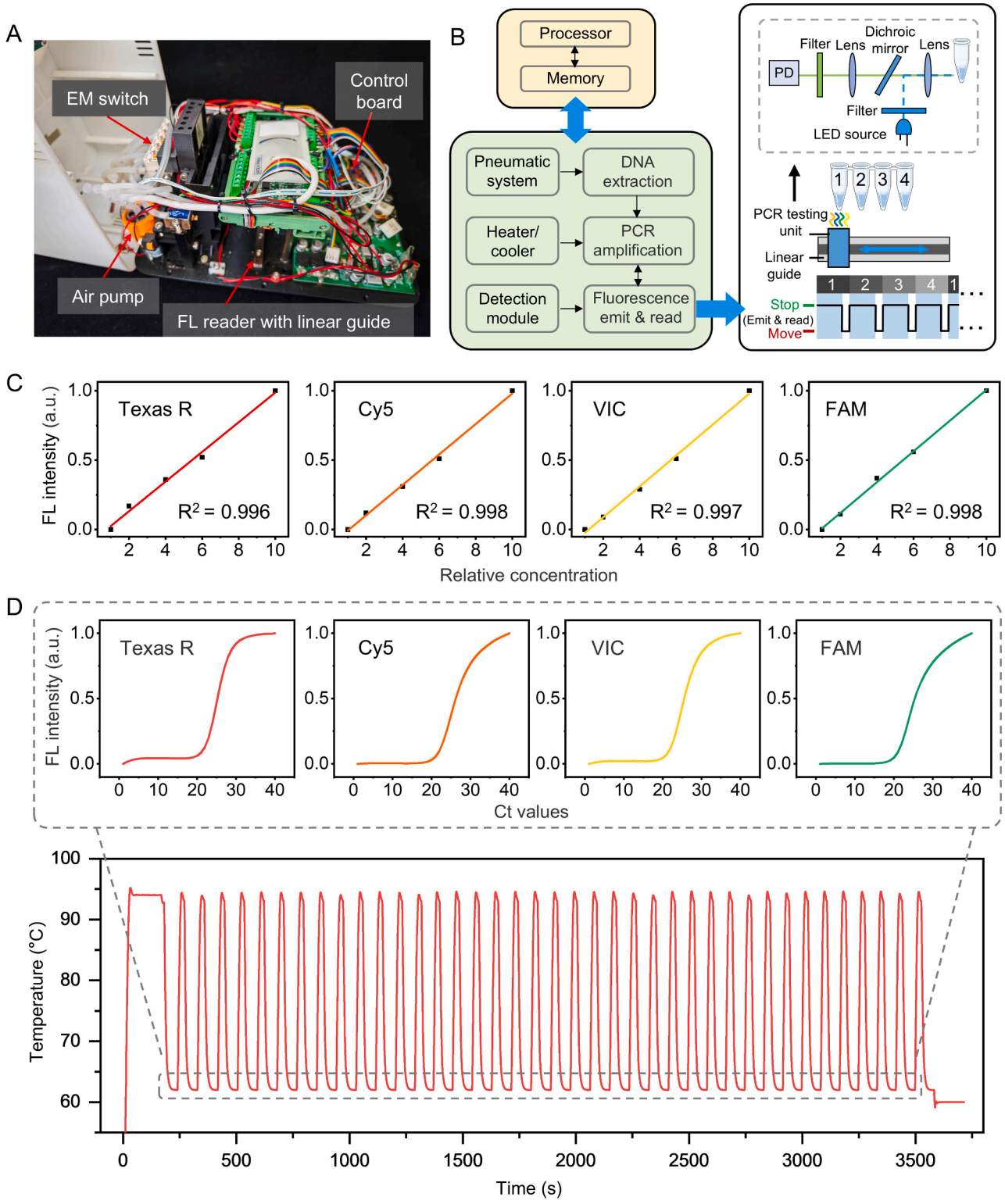

Fig. 4. Characterization of the portable and automated device. (A) Photo of the main components of the device. (B) Flow chart of the relationship of different elements. (C) Regression fit of the relative concentration fluorescence values for Texas R, Cy5, VIC, and FAM detected by the device. (D) Temperature profile for 40 cycles and the representative Ct value versus fluorescence curves recording at the temperature of 62 °C.

to fit the shape of the amplification tube, ensuring precise and uniform heating. To facilitate fluorescence detection, small openings were cut out on both sides of the module. The fluorescence detection module contains a light-gathering lens, filters, LED light sources, a dichroic mirror, and photodiode (PD) signal acquisition modules (Fig. 4B). A front-mounted lens focuses the light to enhance fluorescence intensity. The whole fluorescence detection module is mounted on a linear guide, which stops at an amplification tube to conduct four multiplexed fluorescence detection and moves to the next tube, continuing until all four tubes are measured.

From the results of standard fluorescent dyes with gradient dilution (Fig. 4C), it is evident that each channel displays strong linearity, with a linear range of > 0.99, indicating the module's capability to accurately detect and quantify fluorescence signals, providing a robust platform for qPCR applications. Fig. 4D showed the temperature variation in one of the amplification tubes. It can be observed that the temperature changes remained stable and efficient over 40 thermal cycles. After hardware validation, the signal processing algorithm was optimized to ensure that the Ct values and their distributions from the RFPS-POCT platform were consistent with those from the commercialized Slan 96 Instrument (Fig. 4D).

3.4. "Sample-in-answer-out" process for HPV variants identification

Fig. 5A showed the reagent operation processes for qPCR using the RFPS-POCT platform. The DNA extraction steps are as follows: (a) Lysis step: A 200 μL sample was pipetted into the lysis chamber and released into the reaction chamber together with the lysis solution under pressure P_1 (= 23 kPa). Air pressure P_2 (= 2.5 kPa) was applied through mixing channel at the bottom of the chamber, achieving a full mixing in about 4 s. An electromagnet was used to extract the microbeads, followed by a pressure P_3 (= 3.5 kPa) through pushing channel to transfer the reagents to the waste chamber. (b) Washing step 1: Washing solution A from washing1 chamber was released to the reaction chamber using pressure P_1. Vortex mixing process was then performed, and the solution was transferred to the waste chamber, with the microbeads extracted in the reaction chamber by the electromagnet. (c) Washing step 2 is similar to washing step 1. It should be noted that each step for washing 1 and 2 was performed two times. (d) Drying step: a pressure of 35 kPa was applied to the microbeads in the reaction chamber through mixing channel for 20 s. It can be clearly observed that there were washing solution residual remaining in the microbeads without drying. (e) Elution step: The elution reagent was injected and mixed in the same way as in previous steps. Since the elution reagent was transferred to the amplification tubes, both P_4 and P_5 (= 35 kPa) were applied at the same time to reach the critical pressure of the lever and seal the amplification tubes. Thus, all the elution reagents were equally distributed to the four amplification tubes for eliciting a multiplex PCR reaction. (f) Paraffin oil sealing step: a pressure of 30 kPa was applied for releasing the paraffin oil to the reaction chamber. It should be noted that the pressure of 30 kPa is higher than the pressure applied in other chambers (23 kPa), due to the high viscosity of paraffin oil. Then P_6 from pushing channel and P_7 from mixing channel (= 40 kPa) were applied simultaneously to transfer the paraffin oil to amplification tubes. Finally, a pressure of 4.5 kPa was applied from the pushing channel to direct the remaining paraffin oil in the reaction chamber to the waste chamber. The paraffin oil sealing step is critical for preventing the evaporation of reagents in amplification tubes and waste chamber during thermal cycles. The detailed information for reagents volume and operation time is provided in Fig. 5B. The whole reagents operation video is provided in Movie S3. After the reagent operation processes, the thermal cycling (thermal profile are provided in Fig. 4D) and fluorescence detection are automatically performed by the benchtop device.

Supplementary material related to this article can be found online at doi:10.1016/j.snb.2026.140134.

3.5. Clinical validation of the POCT platform

To evaluate RFPS-POCT's clinical applicability, we tested 53 cervical swab samples from volunteers. Each patient sample was split into two aliquots: one aliquot was processed using the RFPS-POCT and the other with a benchtop PCR system (SLAN-96P, China) (Fig. 6A). The standard qPCR procedure involves manually reagent transferring, centrifugal mixing and drying steps, which takes about 30 min. Thanks to the automatic pneumatic microfluidic manipulation and efficient bubble mixing, the RFPS cartridge only takes less than 3 min to complete the purification procedure (Fig. 5B). On the other hand, due to the fast heating/cooling strategy used in the fluorescence detection device, the heating and cooling time takes about 12 s and 26 s, respectively, making the whole qPCR procedure about 60 min (Fig. 4D) and it is much faster than that of the commercial fluorescence detection equipment (about 120 min) we used in the experiments. Both assays used the same purification and testing reagents. Fig. 6B shows the results from RFPS-POCT and conventional qPCR. We compared fluorescence intensity, where a good concordance between these two methods was observed with the Pearson coefficient (r) values of 0.94. As independent analytical measures, the fluorescence intensity (FL) distribution is provided for both positive and negative samples (Fig. 6C). The FL values were significantly higher in patients with HPV than those in negative groups (Fig. 6D). HPV 18 genotypes ($n = 13$) prevailed in the 53 samples and HPV 66/68 accounted for only one case in the tested samples. Some patients were infected by more than one types of HPV, for example, No. 39 patient was infected by both HPV 18 and HPV 51. One case of false negative for HPV 18 and one case of false positive for HPV 45 were observed, achieving a sensitivity of 96.4% and a specificity of 96% (Figs. 6E and 6F). Receiver operating characteristic (ROC) curves were further constructed for IBV. We found the diagnostic accuracy was excellent, with an area under the curve of 0.998 (Fig. 6G). The video of the "sample-in-answer-out" performance is provided in Movie S4.

Supplementary material related to this article can be found online at doi:10.1016/j.snb.2026.140134.

4. Conclusion

In this study, we developed a portable and automated platform capable of discriminating fifteen HPV genotypes, covering all fourteen high-risk types and one possible high-risk type. The system consists of a palm-sized cartridge and a compact benchtop fluorescence detection device. At its core is the rigid–flexible pneumatic switching (RFPS) technology, which self-regulates critical pressure to control reagent flow without the need for additional pneumatic channels. This not only simplifies the design and improves robustness but also reduces the material cost to about $1.2 (Supplementary Table 1). The RFPS cartridge integrates multiple essential functions, including omnidirectional dispensing, on-demand release, vortex mixing, and, importantly, long-term reagent storage, a feature rarely achieved in existing POCT devices. The benchtop device further streamlines multiplexed fluorescence detection by replacing multiple modules with a single movable unit for 4×4 qPCR, shrinking the entire system to the size of a shoebox and making it suitable for point-of-care deployment. Using this platform, fifteen HPV genotypes were reliably detected with limits of detection ranging from 3 to 50 copies/μL. Clinical validation with 53 cervical swab samples demonstrated actual "sample-in-answer-out" performance within one hour, showing strong agreement with a gold-standard analyzer ($r = 0.94$), and achieving 96.4% sensitivity and 96% specificity. Overall, the platform fulfills WHO's ASSURED criteria for point-of-care diagnostics. Beyond HPV screening, the RFPS-based approach offers a versatile foundation for a broad range of applications, including biomedical testing, environmental monitoring, food safety, material synthesis, and pharmaceutical analysis.

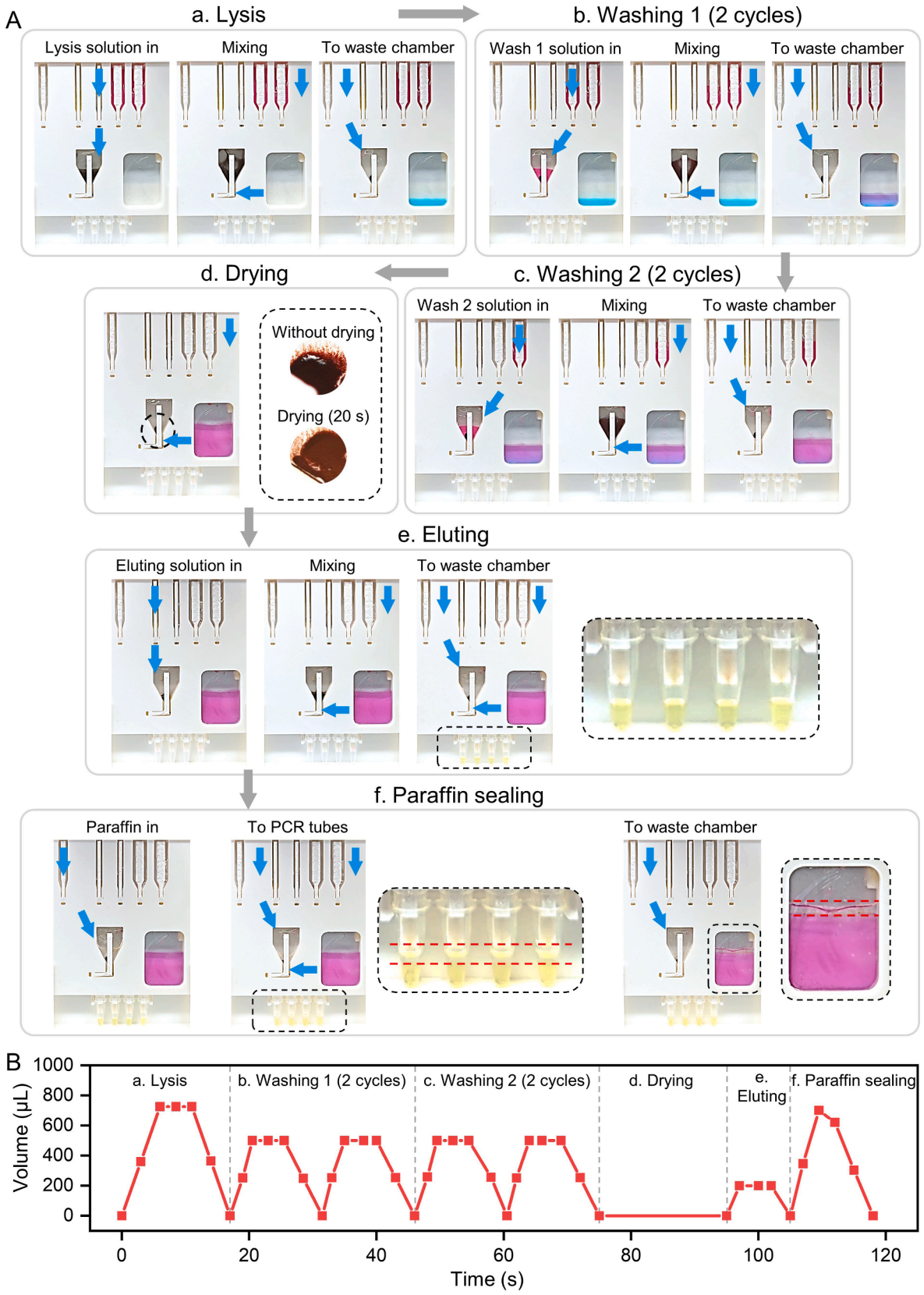

Fig. 5. Work principle by using the RFPS cartridge. (A) Pictures illustrating the whole process of DNA purification process including lysis, washing 1 (2 cycles), washing 2 (2 cycles). drying, eluting, and paraffin sealing. (B) The relationship between the liquid volume in the reaction chamber and the operation time.

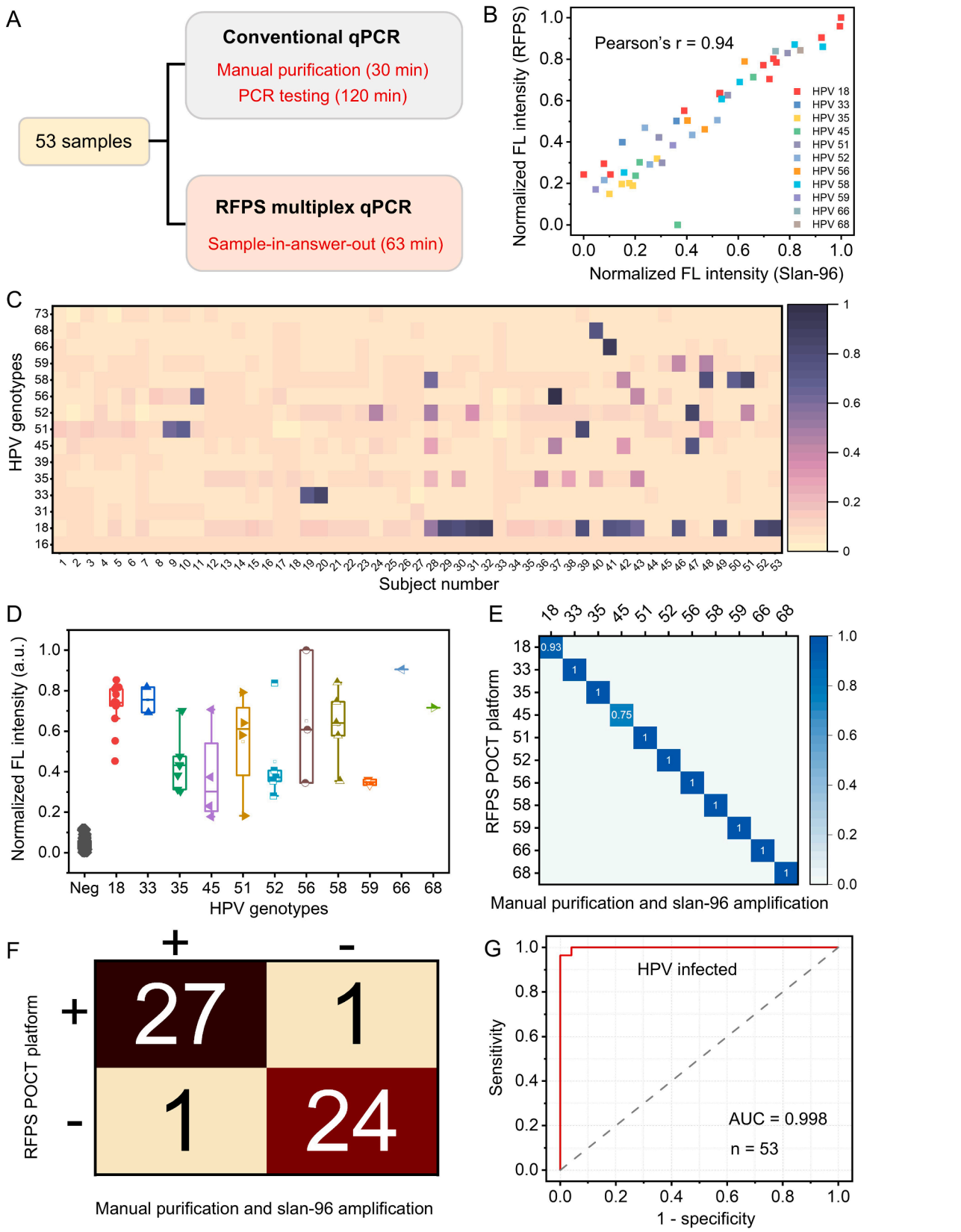

Fig. 6. Testing of clinical samples with RFPS platform for HPA variants identification. (A) Clinical study design. A total of 53 samples were analyzed by the platform and conventional qPCR, including 28 patients' samples and 25 control individuals without HPV. (B) Evaluation of concordance between RFPS-POCT qPCR and conventional qPCR. The results showed a positive correlation (Pearson's r = 0.94). (C) Heat map discriminating the 15 types of HPV variants in the clinical samples. (D) FL intensity of the identified HPV variants and negative controls. (E) Confusion matrix showing the HPV variant identification results for RFPS-POCT platform and conventional qPCR (using manual purification and slan-96 for amplification). (F) Sensitivity concordance between RFPS-POCT qPCR and qPCR, where qPCR results with Ct value > 38 were identified as negative. (G) ROC curves. The AUC was 0.998 for HPV positive samples.

CRediT authorship contribution statement

Chao Liang: Writing – review & editing, Project administration, Methodology, Funding acquisition, Conceptualization. **Jingyang Zhao:** Writing – original draft, Visualization, Investigation, Formal analysis, Data curation. **Yingjun Xiao:** Writing – original draft, Investigation, Formal analysis. **Hanqing Jiang:** Writing – review & editing, Project administration, Funding acquisition. **Jiajun Li:** Investigation, Formal analysis.

Funding

This work was supported by the Natural Science Foundation of Hangzhou (grant 2024SZRYBH180012) and the National Natural Science Foundation of China (grant 12350003).

Declaration of Competing Interest

The authors declare that they have no known competing financial interests or personal relationships that could have appeared to influence the work reported in this paper.

Acknowledgments

We acknowledge the Research Center for Industries of the Future (RCIF) at Westlake University and the Westlake Education Foundation for their support of this work.

Declaration of competing interest

The authors declare that they have no competing interests.

Appendix A. Supporting information

Supplementary data associated with this article can be found in the online version at doi:10.1016/j.snb.2026.140134.

Data availability

Data will be made available on request.

References

[1] H. Sung, J. Ferlay, R.L. Siegel, M. Laversanne, I. Soerjomataram, A. Jemal, F. Bray, CA Cancer J. Clin. 71 (2021) 209–249, https://doi.org/10.3322/caac.21660.
[2] J.M.M. Walboomers, M.V. Jacobs, M.M. Manos, F.X. Bosch, J.A. Kummer, K. V. Shah, P.J.F. Snijders, J. Peto, C.J.L.M. Meijer, N. Muñoz, J. Pathol. 189 (1999) 12–19, https://doi.org/10.1002/(SICI)1096-9896(199909)189:1<12::AID-PATH431>3.0.CO;2-F.
[3] A.A. McBride, Nat. Rev. Microbiol 20 (2022) 95–108, https://doi.org/10.1038/s41579-021-00617-5.
[4] E.J. Crosbie, M.H. Einstein, S. Franceschi, H.C. Kitchener, Lancet 382 (2013) 889–899, https://doi.org/10.1016/S0140-6736(13)60022-7.
[5] N. Egawa, J. Doorbar, Virus Res. 231 (2017) 119–127, https://doi.org/10.1016/j.virusres.2016.12.017.
[6] Z. Chen, S. Nie, J. Ran, Y. Wang, Q. Li, H. Zhao, X. Chen, D. Xiong, D. Xiao, J. Med. Virol. 96 (2024) e70097, https://doi.org/10.1002/jmv.70097.
[7] S.M. Amaro-Filho, A. Gradissimo, M. Usyk, F.C.B. Moreira, L.M. de Almeida, M.A. M. Moreira, R.D. Burk, Int. J. Cancer 146 (2020) 731–738, https://doi.org/10.1002/ijc.32315.
[8] H. Liu, R. Xu, J. Chen, S. Wang, L. Wang, M. Wu, H. Wang, Infect. Genet. Evol. 130 (2025) 105746, https://doi.org/10.1016/j.meegid.2025.105746.
[9] S. de Sanjose, W.G. Quint, L. Alemany, D.T. Geraets, J.E. Klaustermeier, B. Lloveras, S. Tous, A. Felix, L.E. Bravo, H.R. Shin, C.S. Vallejos, P.A. de Ruiz, M. A. Lima, N. Guimera, O. Clavero, M. Alejo, A. Llombart-Bosch, C. Cheng-Yang, S. A. Tatti, E. Kasamatsu, E. Iljazovic, M. Odida, R. Prado, M. Seoud, M. Grce, A. Usubutun, A. Jain, G.A. Suarez, L.E. Lombardi, A. Banjo, C. Menéndez, E. J. Domingo, J. Velasco, A. Nessa, S.C. Chichareon, Y.L. Qiao, E. Lerma, S. M. Garland, T. Sasagawa, A. Ferrera, D. Hammouda, L. Mariani, A. Pelayo, I. Steiner, E. Oliva, C.J. Meijer, W.F. Al-Jassar, E. Cruz, T.C. Wright, A. Puras, C. L. Llave, M. Tzardi, T. Agorastos, V. Garcia-Barriola, C. Clavel, J. Ordi, M. Andújar, X. Castellsagué, G.I. Sánchez, A.M. Nowakowski, J. Bornstein, N. Muñoz, F. X. Bosch, Retrospective International Survey and HPV Time Trends Study Group, Lancet Oncol. 11 (2010) 1048–1056, https://doi.org/10.1016/S1470-2045(10)70230-8.
[10] P. Jeudin, T. Abebe, R. Butler, D. Hooi, A. Watt, C.D. Capo-Chichi, S. George, C. Ragin, N. McFarlane Anderson, M. Schlumbrecht, JCO Glob. Oncol. 7 (2021) 1206–1208, https://doi.org/10.1200/GO.21.00151.
[11] M. El-Zein, L. Richardson, E.L. Franco, J. Clin. Virol. 76 (2016) S62–S68, https://doi.org/10.1016/j.jcv.2015.11.020.
[12] H. Sohrabi, M.R. Majidi, M. Fakhraei, A. Jahanban-Esfahlan, M. Hejazi, F. Oroojalian, B. Baradaran, M. Tohidast, M. Guardia, A. Mokhtarzadeh, Talanta 243 (2022) 123330, https://doi.org/10.1016/j.talanta.2022.123330.
[13] S. Seely, J.M. Zingg, P. Joshi, B. Slomovitz, M. Schlumbrecht, E. Kobetz, S. Deo, S. Daunert, Anal. Chem. 95 (2023) 13488–13496, https://doi.org/10.1021/acs.analchem.3c01723.
[14] H. Bai, Y. Liu, L. Gao, T. Wang, X. Zhang, J. Hu, L. Ding, Y. Zhang, Q. Wang, L. Wang, J. Li, Z. Zhang, Y. Wang, C. Shen, B. Ying, X. Niu, W. Hu, Biosens. Bioelectron. 248 (2024) 115968, https://doi.org/10.1016/j.bios.2023.115968.
[15] X. Zhao, X. Li, W. Yang, J. Peng, J. Huang, S. Mi, Analyst 146 (2021) 5102–5114, https://doi.org/10.1039/d1an00623a.
[16] J.E. Kreutz, J. Wang, A.M. Sheen, A.M. Thompson, J.P. Staheli, M.R. Dyen, Q. Feng, D.T. Chiu, Lab Chip 19 (2019) 1035–1040, https://doi.org/10.1039/c8lc01223g.
[17] Y.C. Yao, N. Li, L.S. Hu, Y.H. Li, Z. Zhang, Asian Pac. J. Trop. Med. 11 (2018) 141–146, https://doi.org/10.4103/1995-7645.225022.
[18] T. Xu, Y. Zhang, S. Li, C. Dai, H. Wei, D. Chen, Y. Zhao, H. Liu, D. Li, P. Chen, B. F. Liu, Y. Tian, Adv. Sci. 12 (2025) e2414918, https://doi.org/10.1002/advs.202414918.
[19] Y. Cai, L. Zhuang, J. Yu, L. He, Z. Wang, T. Hu, L. Li, X. Li, H. Zhou, X. Huang, Sens. Actuators B Chem. 405 (2024) 135295, https://doi.org/10.1016/j.snb.2024.135295.
[20] Z. Xu, D. Chen, T. Li, J. Yan, J. Zhu, T. He, R. Hu, Y. Li, Y. Yang, M. Liu, Nat. Commun. 13 (2022) 6480, https://doi.org/10.1038/s41467-022-34086-y.
[21] L.A. Fleider, M. de Los Ángeles Tinnirello, F. Gómez Cherey, M.G. García, L. H. Cardinal, F. García Kamermann, S.A. Tatti, PLoS One 18 (2023) e0279728, https://doi.org/10.1371/journal.pone.0279728.
[22] J. Cuzick, A. Szarewski, D. Mesher, L. Cadman, J. Austin, K. Perryman, L. Ho, G. Terry, P. Sasieni, R. Dina, W.P. Soutter, Int. J. Cancer 122 (2008) 2294–2300, https://doi.org/10.1002/ijc.23339.
[23] F.X. Bosch, C. Robles, M. Díaz, M. Arbyn, I. Baussano, C. Clavel, G. Ronco, J. Dillner, M. Lehtinen, K.U. Petry, M. Poljak, S.K. Kjaer, C.J. Meijer, S.M. Garland, J. Salmerón, X. Castellsagué, L. Bruni, S. de Sanjosé, J. Cuzick, Nat. Rev. Clin. Oncol. 13 (2016) 119–132, https://doi.org/10.1038/nrclinonc.2015.146.
[24] World Health Organization. Global prevalence and incidence of selected curable sexually transmitted infections: Overview and estimates. Geneva: WHO, WHO/HIV_AIDS/ 2 ⟨https://apps.who.int/iris/bitstream/handle/10665/66818/WHO_HIV_AIDS_2001.02.pdf⟩ (2001).
[25] S. Augustine, A. Venkadesh, S. Kaushal, E. Lee, M. Ajaj, N.E. Lee, Anal. Chem. 97 (2025) 9569–9599, https://doi.org/10.1021/acs.analchem.4c07075.
[26] S. Yang, P. Sharma, Asme. Appl. Mech. Rev. 75 (2023) 044801, https://doi.org/10.1115/1.4056303.
[27] M.J. Buehler, Asme. Appl. Mech. Rev. 76 (2024) 021001, https://doi.org/10.1115/1.4063843.
[28] M. Yafia, O. Ymbern, A.O. Olanrewaju, A. Parandakh, A. Sohrabi Kashani, J. Renault, Z. Jin, G. Kim, A. Ng, D. Juncker, Nature 605 (2022) 464–469, https://doi.org/10.1038/s41586-022-04683-4.
[29] J. Li, Y. Liu, T. Wu, Z. Xiao, J. Du, H. Liang, C. Zhou, J. Zhou, Nat. Commun. 15 (2024) 5603, https://doi.org/10.1038/s41467-024-49810-z.
[30] L. Zhang, J.Q. Cui, S. Yao, Lab Chip 25 (2025) 175–186, https://doi.org/10.1039/d4lc00800f.
[31] H. Yuan, C. Wan, X. Wang, S. Li, H. Xie, C. Qian, W. Du, X. Feng, Y. Li, P. Chen, B. F. Liu, Small 20 (2024) e2310206, https://doi.org/10.1002/smll.202310206.
[32] L.X. Kong, A. Perebikovsky, J. Moebius, L. Kulinsky, M. Madou, J. Lab Autom. 21 (2016) 323–355, https://doi.org/10.1177/2211068215588456.
[33] M. Tang, X. Huang, Q. Chu, X. Ning, Y. Wang, S.K. Kong, X. Zhang, G. Wang, H. P. Ho, Lab Chip 18 (2018) 1452–1460, https://doi.org/10.1039/c8lc00042e.
[34] Z. Ding, D. Zhang, G. Wang, M. Tang, Y. Dong, Y. Zhang, H.P. Ho, X. Zhang, Lab Chip 16 (2016) 3604–3614, https://doi.org/10.1039/c6lc00542j.
[35] Y. Deng, J. Fan, S. Zhou, T. Zhou, J. Wu, Y. Li, Z. Liu, M. Xuan, Y. Wu, Biomicrofluidics 8 (2014) 024101, https://doi.org/10.1063/1.4867241.
[36] Z. Wang, Y. Wang, L. Lin, T. Wu, Z. Zhao, B. Ying, L. Chang, Biosens. Bioelectron. 195 (2022) 113663, https://doi.org/10.1016/j.bios.2021.113663.
[37] J. Park, D.H. Han, S.H. Hwang, J.K. Park, Lab Chip 20 (2020) 3346–3353, https://doi.org/10.1039/d0lc00432d.
[38] T. Laksanasopin, T.W. Guo, S. Nayak, A.A. Sridhara, S. Xie, O.O. Olowookere, P. Cadinu, F. Meng, N.H. Chee, J. Kim, C.D. Chin, E. Munyazesa, P. Mugwaneza, A. J. Rai, V. Mugisha, A.R. Castro, D. Steinmiller, V. Linder, J.E. Justman, S. Nsanzimana, S.K. Sia, Sci. Transl. Med 7 (2015) 273re1, https://doi.org/10.1126/scitranslmed.aaa0056.
[39] S. Hoang, M. Shehada, K. Karydis, P. Brisk, W.H. Grover, Ann. Biomed. Eng. 53 (2025) 207–216, https://doi.org/10.1007/s10439-024-03628-4.
[40] S. Ahrar, M. Raje, I.C. Lee, E.E. Hui, Sci. Adv. 9 (2023) eadg0201, https://doi.org/10.1126/sciadv.adg0201.
[41] T. Gilet, S. van Loo, Microfluid. Nanofluidics 26 (2022) 20, https://doi.org/10.1007/s10404-022-02524-4.
[42] C. Qian, P. Li, J. Wang, X. Hong, X. Zhao, L. Wu, Z. Miao, W. Du, X. Feng, Y. Li, P. Chen, B.F. Liu, Anal. Chem. 96 (2024) 7145–7154, https://doi.org/10.1021/acs.analchem.4c00651.

[43] X. Chen, T. Li, H. Zeng, Z. Hu, B. Fu, Int J. Heat. Mass Transf. 98 (2016) 131–140, https://doi.org/10.1016/j.ijheatmasstransfer.2016.03.041.
[44] A.D. Stroock, S.K. Dertinger, A. Ajdari, I. Mezic, H.A. Stone, G.M. Whitesides, Science 295 (2002) 647–651, https://doi.org/10.1126/science.1066238.
[45] M. Grumann, A. Geipel, L. Riegger, R. Zengerle, J. Ducrée, Lab Chip 5 (2005) 411–416, https://doi.org/10.1039/b418253g.
[46] J. Park, D.H. Han, S.H. Hwang, J.K. Park, Lab Chip 20 (2020) 3346, https://doi.org/10.1039/d0lc00432d.
[47] S. Burger, M. Schulz, F. von Stetten, R. Zengerle, N. Paust, Lab Chip 16 (2016) 261–268, https://doi.org/10.1039/c5lc01280e.

Jingyang Zhao is currently pursuing the Ph.D. degree at Hanqing Jiang Lab, in joint program of Westlake University and Zhejiang University. He currently engaged in bio-MEMS and microfluidic systems. His research interests include the biosensing technologies, and their applications in disease biomarker detection and organ-on-chip biomedical systems.

Yingjun Xiao is currently working as a technologist at Clinical Laboratory, The Third Affiliated Hospital of Zhejiang Chinese Medical University (Zhejiang Provincial Zhongshan Hospital). Her research interests include clinical laboratory diagnostics, pathogen detection and antimicrobial susceptibility testing, as well as the analysis of metabolic biomarkers and gut microbiota in disease.

Jiajun Li received the M.S. degree in Bioengineering from Shenyang Agricultural University. He is currently a Research Assistant at Hanqing Jiang Lab, Westlake University. His research interests focus on the development of rapid, accurate, and portable diagnostic technologies for disease detection.

Chao Liang received the Ph.D. degree in Mechanical Engineering from Dalian University of Technology. He is currently an associate researcher at Engineering School of Westlake University. His research interests include microfluidic liquid manipulation and the development of point-of-care diagnostic platforms for biomedical and healthcare applications.

Hanqing Jiang received the Ph.D. degree in Mechanics from Tsinghua University. He is currently a Chair Professor and also Vice Dean for Research at Engineering School of Westlake University. His research interests focus on mechanics, flexible and stretchable electronics, metamaterials, and applications in biomedical devices and soft systems.